Publications

6-16-2011

Group Velocity and Energy Flux in the Thermosphere: Limits on the Validity of Group Velocity in a Viscous Atmosphere

R. L. Walterscheid
The Aerospace Corporation

Michael P. Hickey Ph.D.
Embry-Riddle Aeronautical University, hicke0b5@erau.edu

Group velocity and energy flux in the thermosphere: Limits on the validity of group velocity in a viscous atmosphere

R. L. Walterscheid[1] and M. P. Hickey[2]

[1]   The response to wave forcing of finite duration comprises a transient forerunner and the steady state signal (or simply the signal). It is the latter that carries information on the spectral content of the forcing, and the signal velocity is the velocity at which wave energy flows. To the extent that group velocity is a good measure of the energy flow velocity, the ray-tracing formalism is a valid description of signal propagation. We have examined vertical group velocities as a measure of vertical energy flow velocity for gravity and acoustic waves propagating into the dissipative lower thermosphere. We find that the effects of dissipation on gravity waves can cause group velocity to become a meaningless measure of the energy flow velocity. When certain terms originating in the diffusion of heat and momentum are neglected, the validity of group velocity can be extended to F region altitudes. For acoustic waves, group velocity can be a good measure of energy flow velocity throughout the lower thermosphere because acoustic waves are far less subject to dissipation.

Citation: Walterscheid, R. L., and M. P. Hickey (2011), Group velocity and energy flux in the thermosphere: Limits on the validity of group velocity in a viscous atmosphere, *J. Geophys. Res.*, *116*, D12101, doi:10.1029/2010JD014987.

1.   Introduction

[2]   Ray tracing in the thermosphere is done using the eikonal equations in which the movement of wave packets is predicted on the basis of group velocity [*Bertin et al.*, 1978; *Waldock and Jones*, 1984; *Vadas and Fritts*, 2009]. The group velocity is formally the velocity at which the wave number vector is found to be constant (conserved) in a homogeneous system [*Lighthill*, 1978]. It is often identified as the velocity with which energy flows, but this has to be shown for the waves in question [*Walterscheid and Hecht*, 2003]. For many systems of interest, the group velocity is the same as the energy flow velocity [*Lighthill*, 1978; *Walterscheid and Hecht*, 2003]. For highly dispersive waves or strongly dissipating waves, however, the association of group speed can be problematic and, in fact, nonexistent [*Walterscheid and Hecht*, 2003; *Jackson*, 1962; *Thau*, 1974; *Lighthill*, 1965]. When this occurs, ray-tracing methods using group velocity have no meaning.

2.   Theory

[3]   When there is a discrete change in the forcing from one state to another, the response consists of a transient forerunner followed by the steady state signal (or simply the signal) that carries information on the frequency content of

the changed forcing. We consider three measures of wave energy propagation for the latter response: group velocity, signal velocity, and energy flow velocity.

2.1.   The Dispersion Relation

[4]   Let

$$\underline{L}[\boldsymbol{\psi}'] = 0 \qquad (1)$$

be a homogeneous linear system of differential equations, where $\underline{L}$ is a differential matrix operator, $\boldsymbol{\psi}$ is the vector of dependent variables, and primes denote wave quantities. If $\boldsymbol{\varphi}'$ is a waveform solution satisfying (1), then (1) may be transformed into a linear system of algebraic equations

$$\underline{M} \cdot \boldsymbol{\varphi}' = 0, \qquad (2)$$

where $\underline{M}$ is the result of $\underline{L}$ operating on $\boldsymbol{\varphi}'$. We assume solutions locally of the form

$$\boldsymbol{\varphi}' = \boldsymbol{\Phi} \exp i \left(\omega t - kx - ly - \int \mu dz \right), \qquad (3)$$

where ω is wave frequency, t is time, k, l, μ are the x, y, z components of the wave number vector $\boldsymbol{\kappa}$, and x, y, z are the zonal, meridional, and vertical components of the position vector $\mathbf{x}$. The quantity μ is the sum of the vertical wave number m (which may be complex) plus an exponential growth term to be discussed below. The wave number vector exclusive of this growth term is hereafter denoted $\mathbf{k}$. We assume that the basic state has no dependency on time or the horizontal spatial coordinates. The form (3) is arrived at first by means of Fourier transforms over x and y and a

[1]Space Science Applications Laboratory, Aerospace Corporation, Los Angeles, California, USA.
[2]Department of Physical Sciences, Embry-Riddle Aeronautical University, Daytona Beach, Florida, USA.

further transform over t. The form (3) is then obtained by assuming a waveform solution in terms of the yet undetermined fourth wave parameter m.

[5] The requirement that (2) have nontrivial solutions requires that $|\underline{M}| = 0$ and generates the characteristic equation

$$f(\omega, \boldsymbol{\kappa}) = 0. \tag{4}$$

When $\{k, l, \omega\}$ are determined by the forcing, $\mu(\omega, k, l)$ is determined from (4).

[6] The solution for μ has the form $\mu = m + i/2H$, where $H = RT/g$ is scale height and R is the gas constant, T is the temperature, g is gravity, and where m may be complex. The second term on the right gives the well-known growth proportional to the inverse square root of background air density [Hines, 1960].

[7] The terms originating in scale-dependent diffusion in the momentum and heat equations may be conveniently grouped with the local time derivatives. Using the viscous force as an example and ignoring background winds and horizontal variations, this grouping gives

$$\left(\frac{\partial}{\partial t} - \frac{1}{\rho} \frac{\partial}{\partial z} \mu_m \frac{\partial}{\partial z} \right) u', \tag{5}$$

where μ_m is dynamic viscosity, $u = \dot{x}$, ρ is density, overbars refer to basic-state quantities, and primes refer to deviations there from (perturbations) [Landau and Lifshitz, 1987]. To a good approximation, μ_m may be considered constant, and the grouping of the local time tendency and the viscous force gives

$$\left[\frac{\partial}{\partial t} - \nu_m \frac{\partial^2}{\partial z^2} \right] \left(u'' e^{z/2H} \right),$$

where $\nu_m = \mu_m / \overline{\rho}$ is kinematic viscosity. The exponential factor is applied to remove the exponential growth of u' with altitude, whence $u' = u'' e^{z/2H}$. Assuming solutions of the form (3) gives

$$\frac{\partial}{\partial t} - \nu_m \left(-m^2 - i\frac{m}{H} + \frac{1}{4H^2} \right) = i \left[\left(\omega + \frac{\nu_m m}{H} \right) - i\nu_m \left(m^2 - \frac{1}{4H^2} \right) \right], \tag{6}$$

where the operators are applied to doubly primed quantities. For convenience, we assume that the Prandtl number (Pr) is unity. Then if the occurrences of ω in the inviscid heat and momentum equations are replaced with the quantity in the square brackets on the right, this generates the dispersion relation for viscid waves. If the waves are assumed to be anelastic ($\partial \rho'/\partial t = 0$) and ν_m locally constant [Vadas and Fritts, 2005], the same replacement can be made in the dispersion relation for all occurrences of ω.

[8] To obtain a dispersion relation, kinematic viscosity is assumed locally constant [Francis, 1973; Pitteway and Hines, 1963; Hickey and Cole, 1987; Vadas and Fritts, 2005]. It can be shown formally that this is equivalent to assuming that $mH \gg 1$. The density weighting of the dependent variables generates the second and third terms in the parentheses on the left side of (6). However, ν_m goes as $\overline{\rho}^{-1}$ while the density weighting goes only as $\overline{\rho}^{-1/2}$. Thus, if one ignores the dependence of ν_m on density, then, for consistency, one

should also ignore the terms originating in the density weighting. This means one should neglect im/H and $1/4H^2$ in relation to m^2.

[9] For later reference, we denote two subcases for the implementation of (6): full implementation (all terms in (6) retained) and semi-Boussinesq implementation (only the $-m^2$ term in (6) is retained).

[10] The Boussinesq designation refers to the fact that locally constant ν_m implies $m \gg 1/H$, and this is satisfied for Boussinesq waves. The designation "semi" refers to the fact that only (6) is evaluated this way; in all other respects, the wave is non-Boussinesq. This somewhat heuristic approach is justified a posteriori.

[11] For a dissipative system, the vertical wave number $m(\omega, k, l)$ is complex with $m = m_r + im_i$. The real part gives the dispersion relation, and the imaginary part gives exponential decay with altitude due to dissipation [Bowman et al., 1980; Francis, 1973; Hickey and Cole, 1987; Klostermeyer, 1972; Pitteway and Hines, 1963; Volland, 1969; Lindzen, 1981]. For damping due to scale-dependent dissipation, wave modes in addition to acoustic-gravity waves occur (visco-thermo waves) [Bowman et al., 1980; Hickey and Cole, 1987; Klostermeyer, 1972]. For a given mode (e.g., gravity waves transferring energy upward), the real part defines a relation,

$$m_r = \mathrm{M}(z, \omega, k, l), \tag{7}$$

where the dependency on z means we have allowed Φ to be a slowly varying function of altitude z [Lighthill, 1978].

2.2. Measures of Energy Propagation

[12] In this section, we briefly describe three measures of the velocity of energy flow.

[13] 1. Group velocity. The vertical group velocity based on (7) is

$$w_g = (\partial M / \partial \omega)^{-1}_{k,l}. \tag{8}$$

[14] 2. Energy flow velocity. The energy flow velocity is defined as

$$\mathbf{U} = \mathbf{F}/E, \tag{9}$$

where $\mathbf{U} = (U, V, W)$, $\mathbf{F} = (F_x, F_y, F_z)$ is the energy flux, and E is the energy density [Walterscheid and Hecht, 2003; Lighthill, 1978; Mainardi et al., 1992]. The quantities U, V, W are the x, y, z components of $\mathbf{U}$.

[15] 3. Signal velocity. The signal velocity is simply the velocity at which a wave carries information. It is equal to the "front velocity", which is the speed at which the first rise (or any rise or fall) of a pulse travels forward and is necessarily equal to the speed at which energy flows ($\mathbf{u}_s = \mathbf{U}$) [Nimtz, 2004]. In this section, we develop relations for both scale-dependent and scale-independent dissipation.

2.3. Analysis of Model Systems

[16] For simplicity, we examine relations for a hydrostatic nonrotating windless Boussinesq system [Dunkerton, 1981].

$$w'_{zz\tau_\alpha \tau_\beta} + N^2 w'_{xx} = 0, \tag{10}$$

where subscripts here denote partial differentiation, N is the Brunt-Väisälä frequency, and

$$\frac{\partial}{\partial \tau_\alpha} = \frac{\partial}{\partial t} + \alpha, \qquad (11)$$

$$\frac{\partial}{\partial \tau_\beta} = \frac{\partial}{\partial t} + \beta, \qquad (12)$$

and where α and β are dissipation rates defined later.

2.3.1. Scale-Dependent Dissipation

[17] In this section, we examine the wave modes that occur with scale-dependent dissipation and the transformation that occurs when dissipation is dominant. Scale-dependent dissipation may be implemented by replacing α and β according to

$$\alpha = \beta \rightarrow -\nu\frac{\partial^2}{\partial z^2} \rightarrow \nu m^2, \qquad (13)$$

where ν is molecular viscosity or thermal diffusivity, assumed equal ($Pr = 1$). Consistent with the Boussinesq approximation, we assume that ν may be considered locally constant [*Hickey and Cole*, 1987].

[18] Despite the idealized nature of the system defined by (10) and (13), it is still rather formidable, and a further simplification is useful. When only viscosity is operating,

$$(\omega - i\alpha)(\omega - i\beta) \rightarrow \omega\left(\omega + i\nu\frac{\partial^2}{\partial z^2}\right) \rightarrow \omega(\omega - i\nu m^2). \qquad (14)$$

This reduces the order of the dispersion relation and gives

$$i\frac{\nu}{\omega}m^4 - m^2 + m_0^2 = 0. \qquad (15)$$

This is quadratic in m^2 and admits two pairs of solutions: one corresponds to gravity waves modified by viscosity and the other to viscous waves modified by buoyancy [*Hickey and Cole*, 1987; *Bowman et al.*, 1980; *Klostermeyer*, 1972]. Equation (15) is easily solved giving

$$m^2 = m_0^2\left[\frac{1 \pm (1 - 4i\alpha_0/\omega)^{\frac{1}{2}}}{2i\alpha_0/\omega}\right], \qquad (16)$$

where

$$\alpha_0 \equiv \nu m_0^2, \qquad (17)$$

and where m_0 is the lossless value of m, namely,

$$m_0^2 = \frac{N^2}{\omega^2}k^2. \qquad (18)$$

For $\alpha_0/\omega \ll 1$, (16) gives to first order in α_0/ω

$$m^2 = m_0^2\left[1 + i\frac{\alpha_0}{\omega}\right] \qquad (19)$$

for the gravity wave solution. For large α_0/ω, the dispersion relation is radically changed. In the large α_0/ω limit, (16) gives

$$m^2 = \pm m_0^2\left[\left(i\frac{\omega}{\alpha_0}\right)^{\frac{1}{2}}\right], \qquad (20)$$

where the plus sign refers to the solution of the dispersion relation that is continuous with (19) (gravity waves) and the minus sign refers to viscous waves. Thus, the gravity wave solution differs from the viscosity wave solution only by a constant factor.

[19] The nature of the gravity wave solution is radically changed depending on whether α_0/ω is small or large. When thermal conduction is included, the order of the equations is raised to third order in m^2. The additional solutions correspond to a pair of thermal conduction waves [*Bowman et al.*, 1980; *Hickey and Cole*, 1987; *Klostermeyer*, 1972]. The addition of thermal conduction with Prandtl number 1 changes the exponent in (20) to 1/3. It does not change the basic result that all modes exhibit similar behavior when $\alpha_0/\omega \gg 1$. The mode of energy transfer is radically different when $\alpha_0/\omega \gg 1$ being primarily by diffusive fluxes rather than by pressure working.

[20] It seems unlikely that gravity wave packets could be maintained in the large α_0/ω limit because of extreme wave dispersion, and although a dispersion relation is defined for these waves, it is unlikely that the group velocity calculated from relations like (20) has any physical significance.

2.3.2. Analysis of Group and Energy Flow Velocities for Scale-Independent Dissipation

[21] The simplest implementation of scale-independent dissipation is Rayleigh friction and Newtonian cooling with constant coefficients α and β, respectively. We use this model to illustrate the difference between the various measures of energy flux velocity. Equation (10) gives the complex dispersion relation

$$m^2 = \frac{\omega^2}{(\omega - i\alpha)(\omega - i\beta)}m_0^2. \qquad (21)$$

With $\alpha = \beta$

$$m^2 = \frac{\omega^2}{(\omega - i\alpha)^2}m_0^2 \qquad (22)$$

and gives

$$m = \pm m_0\frac{\omega}{\alpha^2 + \omega^2}(\omega + i\alpha). \qquad (23)$$

The real part of m is

$$m_r = \pm m_0\frac{\omega^2}{\omega^2 + \alpha^2}. \qquad (24)$$

The imaginary part is

$$m_i = \pm m_r\alpha/\omega. \qquad (25)$$

In the limit of large dissipation, both m_r and m_i tend to zero, albeit m_i more slowly. The vertical wavelength becomes very long, and the attenuation rate diminishes.

2.3.2.1. Group Velocity

[22] The group velocity is obtained from the real part of the complex dispersion relation (23) giving

$$w_g = -\frac{\omega}{m_r}\frac{\omega^2 + \alpha^2}{\omega^2 - \alpha^2}, \qquad (26)$$

which is singular when $\omega = \alpha$.

2.3.2.2. Signal Velocity

[23] We derive the signal velocity w_s for the case of scale-independent diffusion for $\alpha = \beta$. The solution is found using the saddle-point method applied to the Laplace transform inversion. The details are given in Appendix A. The vertical signal velocity is

$$w_s = -\frac{\omega}{m_r} \tag{27}$$

where m_r is given by the real part of (16).

[24] Comparing (27) to (26), we see that the two expressions differ markedly as α/ω becomes order unity.

2.3.2.3. Energy Flow Velocity

[25] The energy flow velocity W is found following *Lighthill* [1978] and *Walterscheid and Hecht* [2003], whence

$$W = -\frac{\omega}{m_r}, \tag{28}$$

where again m_r is the real part of (16). The derivation of (28) is given in Appendix B. We have confirmed the equality of the signal and energy flow velocity. Equations (26), (27), and (28) imply that the group velocity becomes a grossly inaccurate measure of energy flow when dissipation is large.

2.4. The Transient Forerunner

[26] As mentioned earlier, a discrete change in the forcing generates a transient forerunner. The transient forerunner for a Boussinesq system propagates as a dispersed group covering an ever increasing interval with ever decreasing amplitude, diminishing as $t^{-3/2}$ [*Thau*, 1974; *Lighthill*, 1965]. With (10) as a model, the saddle-point method gives $\psi \sim e^{-\alpha t} e^{i(\omega_r t - \mathbf{k} \cdot \mathbf{x})}$ for the exponential part of the solution for simple scale-independent dissipation, where $\omega_r = Nk/m$ and m is real [*Thau*, 1974].

[27] Transients differ from the signal in that the dispersive properties of the wave rather than the frequency content of the forcing determine wave frequency. Instead of analyzing with respect to the set $\{k, l, \omega\}$ and solving the characteristic equation for $m(\omega, k, l)$ with frequency given, one analyzes an initial disturbance with respect to $\{\mathbf{k}\}$ and solves the characteristic equation for frequency with $\mathbf{k}$ given, whence $\omega = \omega(\mathbf{k})$.

[28] Whereas it is natural to allow $m(\omega, k, l)$ to be complex when $\{k, l, \omega\}$ are real Fourier coordinates, it is natural to allow ω to be complex when $\mathbf{k}$ is real. With complex ω, the model system (10) with $\alpha = \beta$ gives $\omega_i = \alpha_0$ and $\omega_r = Nk/m$. This gives the exponential form of damped transients in the preceding paragraph. The value of ω for every $\mathbf{k}$ defining the initial disturbance $\psi(\mathbf{x}, 0) = \int \psi_{\mathbf{k}} e^{i\mathbf{k} \cdot \mathbf{x}} d\mathbf{k}$ may be similarly expressed.

[29] A rigorous theory for wave packet propagation for damped waves is formidable. The propagation of an initial disturbance where the damping rate is given as the imaginary part of complex frequency has been studied by a number of authors [*Lighthill*, 1965; *Muschietti and Dum*, 1993; *Mainardi et al.*, 1992]. The validity of group velocity is not affected by a small amount of dissipation. *Lighthill* [1965] noted, however, that when the dissipation rate is comparable to the wave frequency, the theory of group velocity is greatly affected [*Thau*, 1974; *Stratton*, 1941].

2.5. The Vadas-Fritts Formalism

[30] *Vadas and Fritts* [2005] (hereafter denoted VF05) developed an approach to wave propagation and decay wherein ω rather than m is complex; damping is in time rather than in height. Solutions damping in time are found by assuming solutions of the form $\psi = A e^{-\omega_i t} e^{i(\omega_r t - \mathbf{k} \cdot \mathbf{x})}$, where ω_r is the real part of complex frequency and ω_i is the imaginary part and contains all of the terms originating in scale-dependent dissipation that contribute to damping (these are the real terms on the right of (6)).

[31] The resemblance of the exponential part of the solution for transients (the solution exclusive of dispersive attenuation) to the VF05 waveform suggests a strong connection to transients. The discussion in section 2.4 suggests that the propagation of an initial disturbance may be analyzable in terms of the VF05 waveforms.

3. Group Velocity and Energy Flow Calculations

[32] In this section, we describe calculations of the vertical group velocity using dispersion relations and direct calculations of the energy flow velocity using our full-wave model (FW).

3.1. Group Velocity

[33] We now examine group velocity with more general models. Group velocity calculations were performed using the dispersion relations of *Hines* [1960] modified to include the effects of nonisothermality in the evaluation of the Brunt-Väisälä frequency [*Einaudi and Hines*, 1971, hereafter denoted EH71] and dispersion relations based on the full-wave model described below. The EH71 relation is nondissipative and is used for reference.

3.1.1. The Full-Wave-Based Dispersion Relation

[34] The full-wave model described in more detail below is a linear, steady state model that describes the vertical propagation of acoustic-gravity waves in an atmosphere with molecular viscosity, thermal conduction, ion drag, Coriolis force, and realistic basic-state wind and temperature profiles. The full-wave model equations can be put in the form (2). In this work, we have ignored the ion-drag and Coriolis forces, whence the characteristic equation generated by $|\underline{\underline{M}}| = 0$ is a third-order equation in m^2. There are three pairs of solutions: a pair of upgoing and downgoing acoustic-gravity waves, a pair of viscosity waves, and a pair of thermal conduction waves [*Hickey and Cole*, 1987; *Bowman et al.*, 1980; *Klostermeyer*, 1972]. The gravity modes are modified by dissipation, and the visco-thermo modes are modified by buoyancy effects. These modes are distinct when dissipation is weak but become similar when dissipation is very strong.

[35] The full-wave-based dispersion equation is solved numerically for m as follows. An initial guess is made, and then the characteristic equation is evaluated through successive iterations using Newton's method until convergence is achieved. The process is started at low altitudes where the effects of dissipation are negligible and where the acoustic-gravity wave roots are given by the adiabatic dispersion equation of EH71. The solution at successively greater

heights is found by initialization with the value of m determined at the previous height.

3.1.2. Group Velocity Calculations

[36] When using the full-wave-based dispersion relation, the group velocity is evaluated by numerical differentiation by calculating the change in m_r with a small change in ω. This approach was validated using the *Hickey and Cole* [1987] model. This model generates a characteristic equation of the same order as the full-wave-based model but otherwise is a simpler model where group velocity can be calculated semianalytically as well as numerically. The quantity m_r is found by taking the real part of the root corresponding to upward propagating gravity waves.

3.2. Energy Flow Velocity

[37] The required quantities are the wave energy fluxes and the wave energy density [*Landau and Lifshitz*, 1987]. These quantities are calculated from the output from the full-wave model.

3.2.1. Full-Wave Model

[38] The full-wave model is a linear, steady state model that describes the vertical propagation of acoustic-gravity waves in an atmosphere with molecular viscosity and thermal conduction, ion drag, Coriolis force, and the eddy diffusion of heat and momentum in the mesosphere. Here we ignore ion drag, the Coriolis force, and eddy diffusion. The model solves the Navier-Stokes equations on a high-resolution grid subject to boundary conditions and allows quite generally for propagation in a height-varying atmosphere (nonisothermal mean state temperature and height-varying mean winds and diffusion). For a prescribed mean state, the wave frequency and horizontal wave number are input and the amplitudes and phases of the perturbations (velocity, temperature, and pressure) are output as a function of height. Other output from the model includes (but is not limited to) energy, momentum and heat fluxes, and energy density. The model has been described by *Hickey et al.* [1997], *Walterscheid and Hickey* [2001], and *Schubert et al.* [2003]. The basic state is defined by the MSIS-90 model [*Hedin*, 1991] evaluated at the equator for a longitude of 105°W and for a UT of 0900 and day number 318. The solar and geomagnetic conditions were assumed to be low, with the daily $F_{10.7}$ = 99, the 81 day mean $F_{10.7}$ = 120, a_p = 38, and year = 1993. For these inputs, the mean exospheric temperature is 877 K. For simplicity, we assume zero background winds. The profiles of background temperature and viscosity used in the model calculations are shown in Figure 1.

[39] The source is defined by a Gaussian heating profile over altitude, with a full-width at half-maximum of 0.125 km. It is centered at an altitude of 10 km. The shape of the amplitude profile and the flux velocities are insensitive to the details of the source. We adjust the source amplitude to give reasonable peak amplitudes.

[40] A Rayleigh-Newtonian sponge layer in addition to natural absorption by viscosity and heat conduction prevents spurious reflection from the upper boundary [*Hickey et al.*, 1997; *Walterscheid and Hickey*, 2001; *Schubert et al.*, 2003]. To increase the relevance to upward propagating wave packets launched by the source, we have used a lower sponge from $z = -400$ km to $z = 0$ to prevent reflection from the lower boundary [*Hickey et al.*, 2000b].

3.2.2. Wave Energy Flux

[41] The total vertical energy flux for a windless background state is

$$\mathbf{F} = \overline{p'\mathbf{u}'} + \overline{\mathbf{v}' \cdot \underline{\sigma}'} + \kappa_m c_p \overline{T} \nabla \overline{\left(T'/\overline{T}\right)^2} \tag{29}$$

and includes the flux due to pressure working (first term on the right), the diffusive flux of kinetic energy (second term), and the diffusive flux of available potential plus elastic energy (third term) [*Landau and Lifshitz*, 1987; *Hickey and Cole*, 1987; *Richmond*, 1983; *Walterscheid and Hecht*, 2003]. Overbars refer to mean values over a wave cycle, and primes refer to deviations there from; $\mathbf{u} = (u, v, w)$ is the velocity vector, $\underline{\sigma}$ is the stress tensor, ρ is air density, c_p is the specific heat at constant pressure, and κ_m is thermal diffusivity.

[42] As the medium becomes increasingly viscous, increasingly more of the energy is carried by the conductive flux of wave energy. At some point, there is a crossover where the conductive flux exceeds the wave energy flux. When this happens, the primary wave is better regarded as a thermo-visco gravity wave. The dispersion relation based on the full-wave model applies to both the high and low dissipation limits.

3.2.3. Wave Energy Density

[43] The wave energy is

$$E = \frac{1}{2}\overline{\rho}\left[\overline{\mathbf{u}^2} + \frac{g^2}{N^2}\overline{\left(\frac{\theta'}{\overline{\theta}}\right)^2} + \frac{1}{c_s^2}\overline{\left(\frac{p'}{\overline{\rho}}\right)^2}\right], \tag{30}$$

where $\theta = T(p_0/p)^\kappa$ is potential temperature, p is pressure, $c_s^2 = \gamma R\overline{T}$ is the sound speed, $N^2 = g\,\partial \log \overline{\theta}/\partial z$ is the Brunt-Väisälä frequency, ρ is density, $\kappa = R/c_p$, and g is gravity-and where $\gamma = c_p/c_\nu$; c_p and c_ν are the specific heats at, respectively, constant pressure and volume; and R is the gas constant for air. The subscript zero refers to a reference value. The fist term on the right is the kinetic energy, the second term is the available potential energy, and the third term is the elastic potential energy [*Walterscheid and Schubert*, 1990].

3.2.4. Calculation of Wave Energy Flux

[44] With F_z and E calculated from the full-wave results, the vertical energy flux velocity is calculated from

$$W = \frac{F_z}{E}. \tag{31}$$

4. Results

[45] We show calculations for a gravity wave that is sufficiently high frequency to propagate well into the lower thermosphere to E region altitudes without severe attenuation and slow enough so that it does not suffer undue reflection (i.e., dispersion relations may be applied). This wave has a horizontal phase speed of 50 m/s, a horizontal wavelength of 60 km, and a period of 20 min. We also perform calculations for an acoustic wave to examine waves where group velocity concepts are likely to remain valid. For consistency with the theoretical treatment, we assume Pr = 1 for calculations based on the full-wave model and the
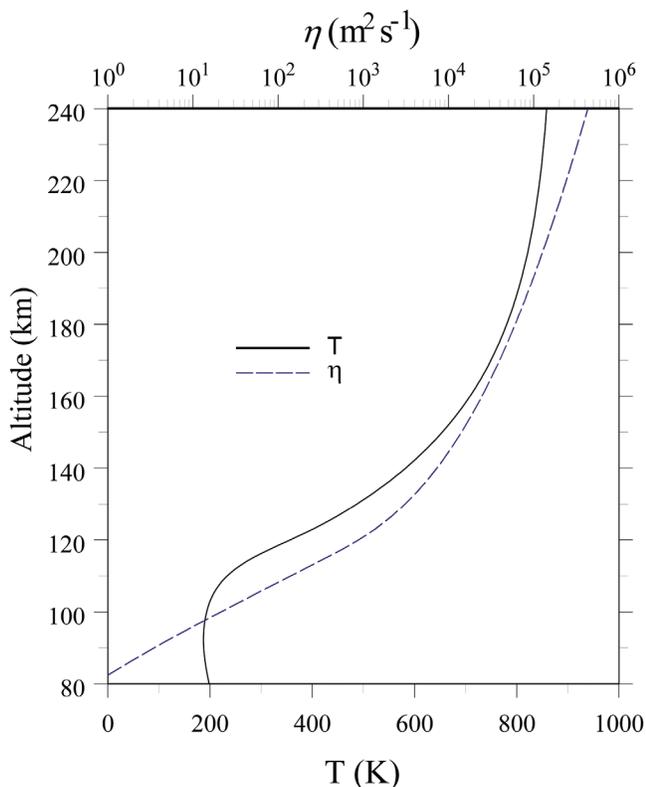
Figure 1. The altitude profile of viscosity and background temperature used for the calculations performed for this study. The source of the profiles is described in the text.

full-wave-based dispersion relation. Results are similar when nominal values of Pr are used.

4.1. Contributions to the Wave Energy Flux

[46] Figure 2 shows the vertical wave energy flow velocity calculated by means of (31) versus altitude for pressure working alone (pressure working term divided by E), for diffusive fluxes alone (diffusive fluxes divided by E), and for the total flux. The diffusive flux contribution grows with altitude. To an altitude of ~130 km, the diffusive flux is negligible compared to the pressure working flux. Near 220 km, the diffusive flux crosses over and is equal to the pressure working flux. Other calculations (not shown) indicate that for slower waves, the diffusive flux can dominate at altitudes well below 200 km, while for faster waves the diffusive fluxes can be a minor contributor at altitudes above those shown.

4.2. Vertical Wave Number

[47] In this section, we compare the vertical wave number based on the full-wave model to the vertical wave number derived from full-wave-based dispersion relations.

[48] The square of the real part of the vertical wave number calculated by means of the full-wave model (FW), two implementations of the full-wave-based dispersion relation, and EH71 are shown in Figure 3. Results for the full-wave-based dispersion relation are shown for the full-implementation of (6) (FWD) and the semi-Boussinesq implementation (FWD/SB). The FW vertical wave number

is obtained by calculating the vertical phase gradient. Above ~130 km, the FW and FWD results begin to diverge from EH71 and show very good agreement with each other, and both lie to the left of EH71. Thus, dissipation increases the vertical scale of the waves. The FWD/SB and EH71 results remain nearly identical until about 170 km where the FWD/SB curve begins to diverge slightly toward longer vertical wavelengths. The disagreement near 115 km between the full-wave and the full-wave-based dispersion relations is due to reflection near the m_r^2 maximum affecting the full-wave results. We remark that close agreement between m_r^2 derived from the FW model and m_r^2 derived from a dispersion relation does not guarantee close agreement between the energy flow velocity W derived from the full-wave model and the group velocity w_g derived from the dispersion relation. The accuracy of the group velocity depends on whether or not the dispersion relation is excessively dispersive.

[49] Also shown is the ratio $\nu(m_0^2 + k^2)/\omega$ relating the rate of wave dissipation to the wave frequency (hereafter denoted η_0). Note that the FWD and FW results begin to depart from the adiabatic EH71 results when $\eta_0 \sim 10^{-1}$ (near 135 km), while the FWD/SB results begin to depart from the EH71 results when $\eta_0 \sim 1$ (near 170 km), more in keeping with theory.

4.3. Group Velocity Versus Energy Flow Velocity

[50] In this section, we compare the energy flow velocity to group velocity for gravity and acoustic waves.
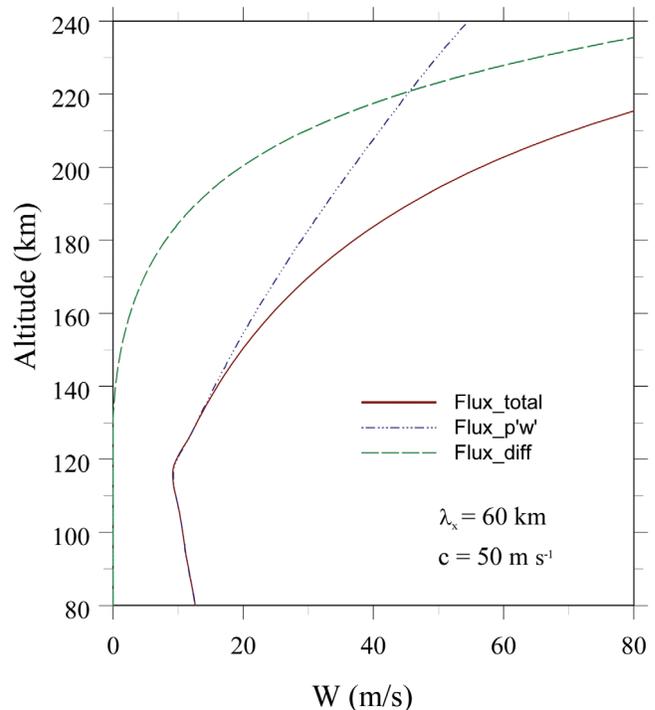

Figure 2. Vertical wave energy flow velocity due to pressure working alone (dash-triple-dotted curve), diffusive fluxes alone (dashed curve), and total (solid curve) versus altitude. Calculations are for wave with a horizontal phase speed of 50 m/s, horizontal wavelength of 60 km, and period of 20 min.
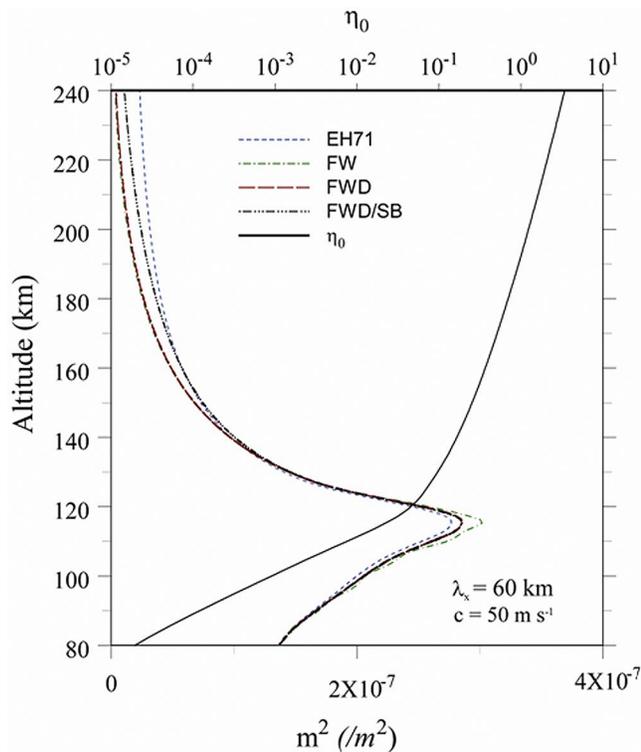
Figure 3. Real part of the vertical wave number calculated by means of the full-wave model (dash-dotted curve), full-wave-based dispersion relation (long-dashed curve), semi-Boussinesq implementation of the full-wave-based relation (dash-triple-dotted curve), and EH71 (short-dashed curve) versus altitude. Also shown is the dissipation parameter η_0 defined in the text (solid curve). The wave is the same as for Figure 2.

4.3.1. Gravity Wave Calculations

[51] Figure 4 shows the group velocity calculated from the EH71, FWD, and FWD/SB dispersion relations and the energy flow velocity W calculated from the FW model output. Also shown is the dissipation ratio η_0. All dissipative results begin to diverge from the adiabatic EH71 results near 130 km. At the same height, the FWD values begin to rapidly diverge from the FW values. The divergence becomes extreme a scale height or two above where the divergence begins. The divergence between the FW and FWD results commence where $\eta_0 \sim 10^{-1}$. In stark contrast, the group velocity based on FWD/SB is virtually the same as the energy flow velocity to altitudes near 190 km, where $\eta_0 \sim 1$. A scale height or two above 190 km, the divergence between the energy flow velocity and the FWD/SB implementation also becomes extreme.

[52] The curves for all dissipative models are to the right of the dissipationless EH71 curve. This is consistent with the corresponding vertical wave numbers and is a reflection of the fact that longer wavelengths tend to be associated with faster group speeds. This is consistent with the result that the semi-Boussinesq implementation FWD/SB gives more realistic values of w_g than the full implementation FWD, since the latter predicts longer vertical wavelengths than the former. Thus, while the full implementation is more

accurate with respect to wavelength, it is less accurate with respect to dispersion.

[53] The validity of a dispersion relation in an inhomogeneous medium depends on the *WKB* criterion being satisfied. This criterion places a constraint on the variation of m compared to m itself. We have evaluated the *WKB* criterion $m_r^{-2}\, dm/dz \ll 1$ and find the *WKB* criterion to be well satisfied [*Walterscheid et al.*, 2000].

4.3.2. Acoustic Wave Calculations

[54] For acoustic waves, the ratio η_0 is smaller than for gravity waves, and the effects of viscosity on group velocity may be minimal. Figure 5 shows w_g calculated from EH71, FWD, and FWD/SB and the full-wave dispersion relation and W calculated from the FW model for an internal acoustic wave with a 2 min period and a phase speed of 1350 $m\ s^{-1}$. (We remark that all internal acoustic waves have phase speeds in excess of the local sound speed but satisfy the physical constraint that the group speed is less the sound speed [*Walterscheid and Hecht*, 2003]). The agreement between all dissipative results is very close except where reflection effects in the FW model cause small departures near 115 km.

[55] Unlike internal gravity waves, faster acoustic waves have shorter vertical wavelengths than slower ones, or alternatively, longer vertical wavelengths are associated with slower speeds. This is reflected in the vertical group velocity where the effect of viscosity in causing vertical wavelengths to increase slows the group velocity.

4.4. Wave Amplitude

[56] In this section, we address the wave amplitude where the group velocity becomes unreliable. Figure 6 shows the amplitude of the vertical velocity perturbation as a function of altitude. Also shown is the ratio η_0. Wave growth peaks near 140 km altitude where the wave attains $\sim$30 m/s. At this point, the wave is close to its breakdown value $u' \sim 50\ m\ s^{-1}$. Where the FWD/SB results for w_g begin to diverge from the energy flux velocity W (near 180 km), the wave amplitude is diminished to approximately one third of its peak value. A scale height or so above, where the divergence becomes extreme, the wave is diminished to $\sim$20% of its peak value (a few m s^{-1}). While the wave is substantially diminished in amplitude from its peak value, it should be able to produce measurable effects. For example, we estimate that an electron density fluctuation of a few percent is attained when the F region bottom side scale height is a few tens of kilometers. We find that the energy and momentum fluxes at these altitudes are not significant.

[57] The waves that are best able to propagate to great altitudes are those that are close to evanescence but not close enough to suffer large wave reflection. These are high-frequency gravity waves with large vertical wavelengths. Figure 7 shows group velocity, energy flux velocity, and the amplitude of w' for the same wave as for Figure 6, but with a 15 min period (67 $m\ s^{-1}$ phase speed). Group velocity is shown for EH71, FWD, and FWD/SB. Again, the FWD/SB results diverge from and remain closer to the FW results until the FWD and FWD/SB results both become highly inaccurate. Wave growth peaks near 160 km altitude where the wave attains $w' \sim 40$ m/s (with $u' \sim 67\ m\ s^{-1}$). This is near where the FWD/SB results for w_g begin to diverge from the FW value of W. A scale height or so higher where the divergence is
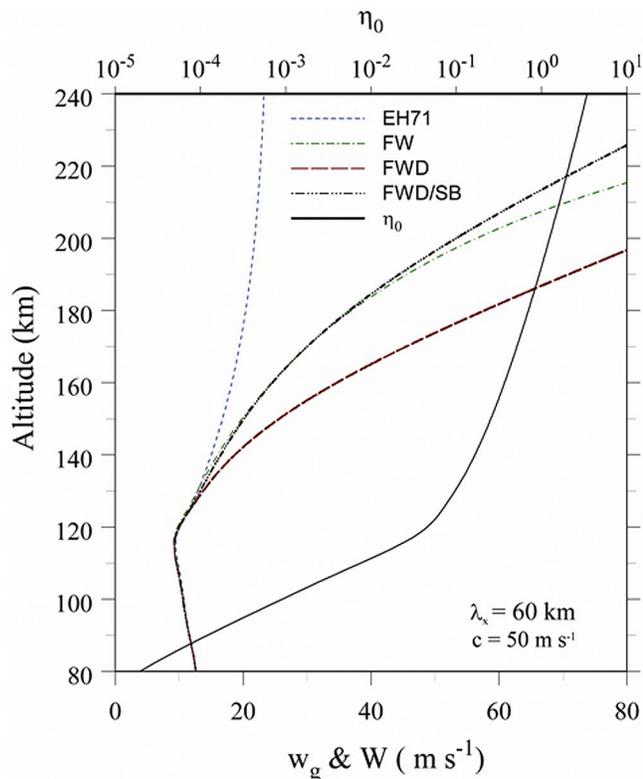
Figure 4. Same as Figure 3 but for the group velocity and the full-wave energy flow velocity.

extreme wave amplitude is not greatly diminished. This wave is clearly able to produce large effects in the ionosphere at altitudes where the group velocity has become a poor indicator of the energy flow.

[58] A large divergence between w_g and W occurs for values of $\eta_0 < 1$ (not shown). The FWD/SB results diverge initially where $\eta_0 \sim 0.2$. A scale height or so higher where the divergence is extreme, $\eta_0 \sim 0.5$. As for the slower wave, the *WKB* criterion is satisfied where a large divergence between w_g and W occurs, being ~ 0.2. Most likely, the fairly early divergence of w_g from W occurs because the group velocity calculations are less robust with respect to the effects of dissipation when the *WKB* criterion begins to approach a significant fraction of unity.

[59] We have also examined slower waves (not shown). For the same wave but with a period of 40 min (phase speed of 25 $m\ s^{-1}$), the wave peaks near 110 km and essentially expires by 140 km, about where group velocity has become meaningless. Waves that are this slow have no significance above the lowest few scale heights of the thermosphere.

[60] For all cases discussed above, the FWD/SB implementation is significantly more accurate than the FWD implementation over a large range of altitudes.

5. Summary and Conclusions

[61] The transient response to sinusoidal forcing of finite duration is a transient forerunner excited by the onset of forcing followed by an upward moving steady state signal in the form of a wave train excited by the forcing over the course of the event. The steady state signal is the dominant

component of the response for $t > z/w_s$, where w_s is the signal (energy flow) speed. Steady state refers to disturbance amplitude at fixed locations; in viscous regions, wave amplitude (energy density) diminishes in time following the signal velocity. For nonsinusoidal forcing, the steady state disturbance may comprise a rich spectrum of waves. The leading edge of the disturbance is determined by the waves with the fastest vertical signal velocity, followed by contributions from slower waves in varying degrees, depending on the spectral content of the forcing.

[62] We have examined the vertical group velocities as a measure of energy flow velocity (signal velocity) for gravity waves propagating into the dissipative lower thermosphere. We find that the effects of dissipation can cause group velocity to become a meaningless measure of energy flow velocity in the lower thermosphere.

[63] We have examined the group velocity for two implementations of wave dissipation: one where all terms are retained and one where only the terms that are consistent with assuming kinematic viscosity locally constant are retained. We denote the latter as the semi-Boussinesq implementation. We find that with the full implementation, the group velocity departs from the energy flow (signal) velocity when the dissipation rate is still small. However, with the semi-Boussinesq implementation, the group velocity can remain a valid measure of energy flow to altitudes where the dissipation rate is very significant and the wave amplitude is greatly diminished.
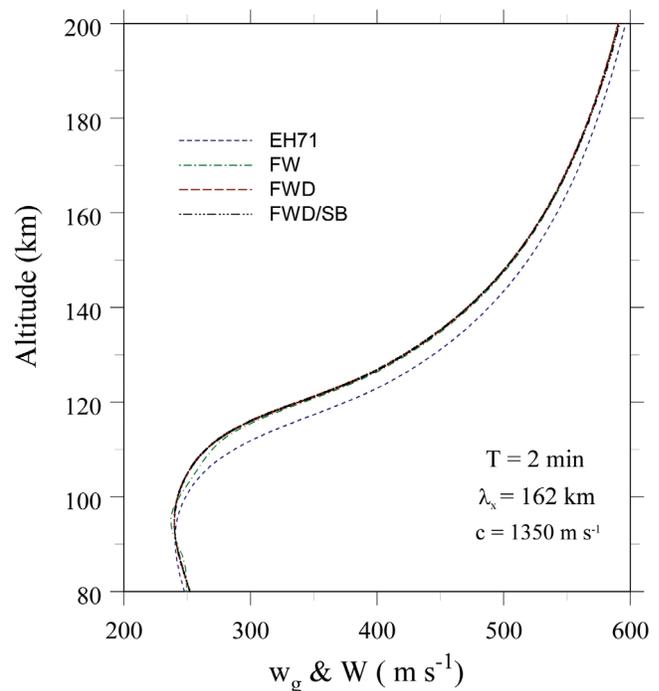

Figure 5. Group velocities for EH71 (short-dashed curve), full-wave-based dispersion relation (dashed curve), full-wave-based dispersion relation with the semi-Boussinesq implementation (dash-triple-dotted curve), and the full-wave energy flow velocity (dash-dotted curve) for an internal acoustic wave with a 2 min period and a phase speed of 1350 $m\ s^{-1}$.
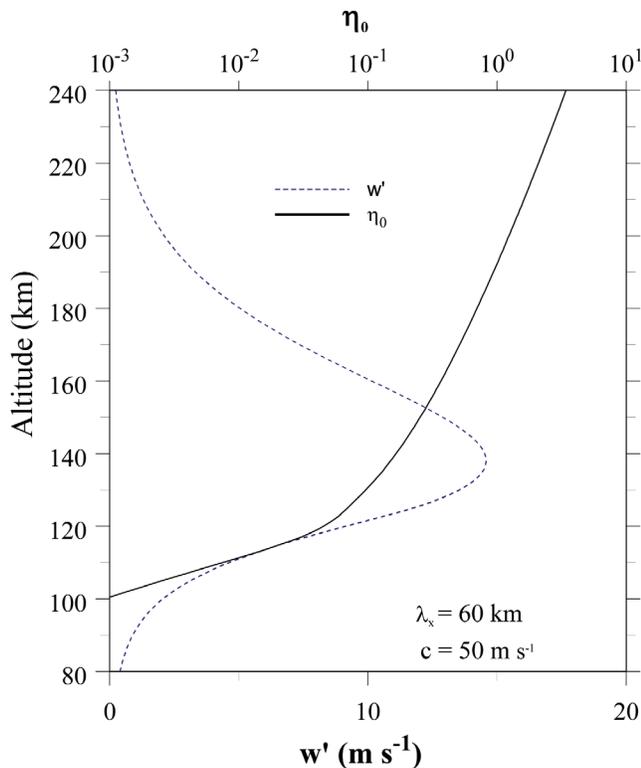
Figure 6. Vertical velocity perturbation (dashed curve) and dissipation ratio η_0 defined in the text (solid curve). The wave is the same as for Figure 2.

[64] We have also calculated group velocity for slower and faster waves. For a 40 min period, the wave expires a few scale heights above the mesopause, about where group velocity is a meaningless measure of the energy flow velocity. Such slow waves are not apt to be significant more than a few scale heights above the mesopause. For a 15 min period, significant wave amplitudes are possible well above where group velocity is meaningless. We conclude that whether group velocity remains valid to altitudes where wave amplitudes are significant can depend sensitively on wave frequency. We find that for all waves considered, the semi-Boussinesq implementation of diffusion is more accurate than the full implementation.

[65] We have noted a resemblance between solutions for the transient forerunner and the form of the solutions assumed by VF05 wherein waves decay locally in time and suggest that the VF05 formalism is suited to the treatment of transients. We have compared our results for the signal to results obtained by *Vadas and Fritts* [2005], *Vadas* [2007], and *Fritts and Vadas* [2008]. Whereas our results show m decreasing and w_g and W increasing with height, the windless results for an isothermal atmosphere shown by these authors show m increasing and w_g decreasing (w_g is deduced from plots of wave packet height versus time). We have calculated m and w_g following VF05, where m is found using their (26) and w_g is found using their (C3). The results (not shown) for the wave used for Figure 2 (m) and Figure 3 (w_g, W) show that at altitudes where dissipation is significant, in contrast to the signal, m is on the high side of the dis-

sipationless EH71 results and w_g is on the low side. The diminishment of the group velocity for the VF05 formalism leads to a turning altitude that is absent from the results for the signal.

[66] We find that for acoustic waves, group velocity can be good measure of energy flow velocity throughout the lower thermosphere. This is because in the lower thermosphere the rate of dissipation compared to wave frequency can be small for acoustic waves.

[67] Our use of steady state theory in the form of the full-wave model is an extension of the use of steady state theory for deriving dispersion relations and group velocities. Full-wave solutions are found by assuming waveform solutions of the form $A_{\omega,k,l}(z) \exp i(\omega t - kx - ly)$ for each dependent variable and solving for $A_{\omega,k,l}(z)$; thus, the full-wave solution is a generalization of solutions where waves of the form $A_{\omega,k,l,m} \exp i(\omega t - kx - ly - mz)$ are assumed: in the full-wave model, the assumption that locally the solutions have the form of plane waves in all three dimensions is relaxed. The full-wave model uses fewer assumptions than *WKB*-based ray-tracing methods. For example, one does not have to resort to assuming that winds, static stability, and viscosity are locally constant. The term "full wave" refers to the fact that full-wave models account for local reflection due to inhomogeneities in the medium (due to, say, thermal gradients and height variable dissipation). This is distinct
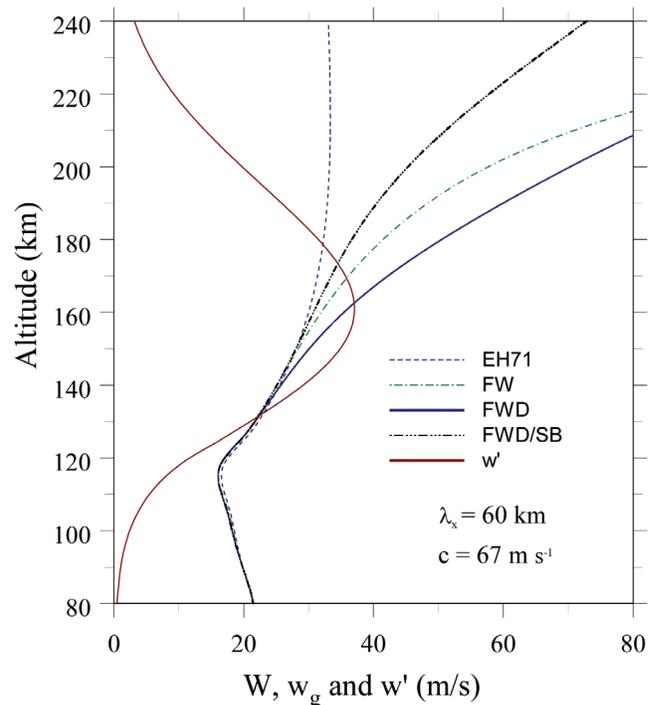

Figure 7. Vertical velocity perturbation (thin solid curve), real part of the vertical wave number calculated by means of the full-wave model (dash-dotted curve), full-wave-based dispersion relation (thick solid curve), semi-Boussinesq implementation of the full-wave-based dispersion relation (dash-triple-dotted curve), and EH71 (dashed curve) versus altitude. The wave is the same as for Figure 2 except that the wave period is 15 min (horizontal phase speed of 67 m s^{-1}).

from partial wave solutions such as *WKB*-based ray tracing where the wave form is purely progressive.

[68] Full-wave models, apart from their usefulness as an extension of *WKB* theory, can exhibit a remarkable amount of realism despite, except perhaps in singular cases, a lack of sustained forcing for long periods of time. This is related first to the fact that the complete linear solution of the response to time-dependent forcing comprises a sum over steady state solutions. This provides the basis for analyzing complex behavior in terms of steady state solutions. Second, the transient response to time-dependent forcing includes finite pulses that satisfy steady state solutions behind the upward propagating wavefront [*Thau*, 1974; *Hickey et al.*, 2000a; *Walterscheid*, 1997]. Steady state relations are found to provide a good description of dissipating waves seen in observations and simulated by time-dependent models. In particular, observations and models generally agree with increasing vertical wavelength for dissipating waves for a variety of wind conditions, including weak winds when Doppler effects that might give a similar effect are minimal or nonexistent [*Hines*, 1968; *Kirchengast et al.*, 1996; *Hocke and Schlegel*, 1996; *Hocke et al.*, 1996; *Oliver et al.* 1997; *Walterscheid et al.*, 2001; *Vadas and Fritts*, 2004; *Yu and Hickey*, 2007; *Miyoshi and Fujiwara*, 2008]. It is also possible that indications of increasing vertical wavelength with height might result from a spectrum of waves that decay locally in time following VF05, or from observational biases arising from the partial sampling of such waves [*Vadas*, 2007].

Appendix A: The Saddle-Point Derivation for Signal Speed for the Model Boussinesq System

[69] A Laplace transform of the time dependency of (10) for a wave of the form

$$w'(x,z,t) = \hat{w}(z,t)\exp(-ikx) \tag{A1}$$

forced at the lower boundary gives the solution

$$\hat{w}(z,t) = \frac{1}{2\pi i}\int_{\gamma-i\infty}^{\gamma+i\infty}\widetilde{w}(s)\exp(zh(s))ds, \tag{A2}$$

where γ lies to the right of all the singularities of the Laplace transform of $\hat{w}(0, t)$ (denoted $\widetilde{w}$) and the singularities of h [*Thau*, 1974]. The function $h(s)$ obtained from transforming (10) is

$$h(s) = \frac{s}{l} - \frac{kN}{s+\alpha}, \tag{A3}$$

where $l = x/t$. Cols (s_0) are found where $h'(s) = 0$ or where

$$h'(s) = 0 = \frac{1}{l} + \frac{kN}{(s+\alpha)^2} \tag{A4}$$

whence

$$s_0 = -\alpha \pm i(lkN)^{\frac{1}{2}}. \tag{A5}$$

The path of integration (steepest descent path) is deformed so that the path through the cols satisfies $\mathrm{Im}(h(s)) = $ constant. For $s = s_0$

$$h(s_0) = -\frac{\alpha}{l} \tag{A6}$$

and thus

$$\mathrm{Im}(h(s_0)) = 0. \tag{A7}$$

Setting $s_0 = i\omega_0$, evaluating $h(i\omega_0)$, and applying (A7) gives

$$l = -\omega_0\frac{\omega_0^2 + \alpha^2}{\omega_0 kN} \tag{A8}$$

and with (26)

$$l = -\frac{\omega_0}{m_r}, \tag{A9}$$

which agrees with (27).

Appendix B: Vertical Energy Flow Velocity for the Model Boussinesq System

[70] The model hydrostatic Boussinesq system is given by

$$\left(\frac{\partial}{\partial t} + \alpha\right)u' = \frac{\partial}{\partial x}\pi', \tag{B1}$$

$$g\frac{\rho'}{\overline{\rho}} = -\frac{\partial}{\partial z}\pi', \tag{B2}$$

$$\left(\frac{\partial}{\partial t} + \alpha\right)g\frac{\rho'}{\overline{\rho}} - w'N^2 = 0, \tag{B3}$$

$$\frac{\partial}{\partial x}u' + \frac{\partial}{\partial z}w' = 0, \tag{B4}$$

where

$$\pi' = \frac{p'}{\overline{\rho}}. \tag{B5}$$

The wave energy derived from this set is

$$E = \frac{1}{2}\left[\overline{u'^2} + \frac{g^2}{N^2}\overline{\left(\frac{\rho'}{\overline{\rho}}\right)^2}\right], \tag{B6}$$

where the first term is kinetic energy and the second is available potential energy. The Brunt-Väisälä frequency (assumed constant) for this system is

$$N^2 = -g\frac{\partial\log\overline{\rho}}{\partial z}. \tag{B7}$$

Following *Walterscheid and Hecht* [2003], each term in (B6) may be related to π'. Multiplying (B1) by u' and (B2) by $\rho'/\overline{\rho}$ and evaluating (B6) gives

$$E = \frac{1}{2}\frac{|m|^2}{N^2}|\hat{\pi}|^2, \tag{B8}$$

where $\hat{\pi}$ is the complex amplitude of π'. The vertical wave energy flux for this system is

$$F_z = \overline{\pi' w'}. \tag{B9}$$

Using (B2) and (B3), it is found that

$$w' = \frac{1}{N^2} (i\omega + \alpha) im\pi'. \tag{B10}$$

Multiplication by π' and averaging gives

$$F_z = \frac{1}{2} \frac{k}{N} |\hat{\pi}|^2 \tag{B11}$$

with the use of (23) and (24). Evaluation of

$$W = \frac{F_z}{E} \tag{B12}$$

gives

$$W = -\frac{\omega}{m_r}. \tag{B13}$$

References

Bertin, F., J. Testud, L. Kersley, and P. R. Rees (1978), The meteorological jet stream as a source of medium-scale gravity waves in the thermosphere: An experimental study, *J. Atmos. Terr. Phys.*, *40*(10–11), 1161–1183, doi:10.1016/0021-9169(78)90067-3.

Bowman, M. R., L. Thomas, and R. H. Thomas (1980), The propagation of gravity waves through a critical layer for conditions of moderate wind shear, *Planet. Space Sci.*, *28*, 119–133, doi:10.1016/0032-0633(80)90088-4.

Dunkerton, T. J. (1981), Wave transience in a compressible atmosphere Part I: Transient internal wave, mean-flow interaction, *J. Atmos. Sci.*, *38*, 281–297, doi:10.1175/1520-0469(1981)038<0281:WTIACA>2.0.CO;2.

Einaudi, F., and C. O. Hines (1971), WKB approximation in application to acoustic-gravity waves, *Can. J. Phys.*, *48*, 1458–1471.

Francis, S. H. (1973), Acoustic-gravity modes and large-scale traveling ionospheric disturbance of a realistic dissipative atmosphere, *J. Geophys. Res.*, *78*, 2278–2301, doi:10.1029/JA078i013p02278.

Fritts, D. C., and S. L. Vadas (2008), Gravity wave penetration into the thermosphere: Sensitivity to solar cycle variations and mean winds, *Ann. Geophys.*, *26*, 3841–3861, doi:10.5194/angeo-26-3841-2008.

Hedin, A. E. (1991), Extension of the MSIS thermosphere model into the middle and lower thermosphere, *J. Geophys. Res.*, *96*, 1159–1172, doi:10.1029/90JA02125.

Hickey, M. P., and K. D. Cole (1987), A quartic dispersion equation for internal gravity waves in the thermosphere, *J. Atmos. Terr. Phys.*, *49*, 889–899, doi:10.1016/0021-9169(87)90003-1.

Hickey, M. P., R. L. Walterscheid, M. J. Taylor, W. Ward, G. Schubert, Q. Zhou, F. Garcia, M. C. Kelley, and G. G. Shepherd (1997), Numerical simulations of gravity waves imaged over Arecibo during the 10-day January 1993 campaign, *J. Geophys. Res.*, *102*, 11,475–11,489, doi:10.1029/97JA00181.

Hickey, M. P., R. L. Walterscheid, and P. G. Richards (2000a), Secular variations of atomic oxygen in the mesopause region induced by transient gravity wave packets, *Geophys. Res. Lett.*, *27*(21), 3599–3602, doi:10.1029/2000GL011953.

Hickey, M. P., R. L. Walterscheid, and G. Schubert (2000b), Gravity wave heating and cooling in Jupiter's thermosphere, *Icarus*, *148*, 266–281, doi:10.1006/icar.2000.6472.

Hines, C. O. (1960), Internal atmospheric gravity waves at ionospheric heights, *Can. J. Phys.*, *55*, 441–445.

Hines, C. O. (1968), An effect of molecular dissipation in upper atmospheric gravity waves, *J. Atmos. Terr. Phys.*, *30*, 845–849, doi:10.1016/S0021-9169(68)80036-4.

Hocke, K., and K. Schlegel (1996), A review of atmospheric gravity waves and traveling ionospheric disturbances: 1982–1995, *Ann. Geophys.*, *14*, 917–940.

Hocke, K., K. Schlegel, and G. Kirchengast (1996), Phases and amplitudes of TIDs in the high latitude F-region observed by EISCAT, *J. Atmos. Terr. Phys.*, *58*, 245–255, doi:10.1016/0021-9169(95)00033-X.

Jackson, J. D. (1962), *Classical Dynamics*, 848 pp., Wiley-Interscience, New York.

Kirchengast, G., K. Hocke, and K. Schlegel (1996), The gravity wave-TID relationship: Insight via theoretical model-EISCAT data comparison, *J. Atmos. Terr. Phys.*, *58*, 233–243, doi:10.1016/0021-9169(95)00032-1.

Klostermeyer, J. (1972), Influence of viscosity, thermal conduction, and ion drag on the propagation of atmospheric gravity waves in the thermosphere, *Z. Geophys.*, *38*, 881–890.

Landau, L. D., and E. M. Lifshitz (1987), *Fluid Mechanics*, 2nd ed., Pergamon, Oxford, U. K.

Lighthill, J. (1965), Group velocity, *IMA J. Appl. Math.*, *1*(3), 269–306, doi:10.1093/imamat/1.3.269.

Lighthill, J. (1978), *Waves in Fluids*, 504 pp., Cambridge Univ. Press, Cambridge, UK.

Lindzen, R. S. (1981), Turbulence and stress due to gravity waves and tidal breakdown, *J. Geophys. Res.*, *86*, 9707–9714, doi:10.1029/JC086iC10p09707.

Mainardi, F., D. Tocci, and F. Tampieri (1992), On energy propagation for internal waves in dissipative fluids, *Nuovo Cimento B*, *107*, 1337–1342, doi:10.1007/BF02726099.

Miyoshi, Y., and H. Fujiwara (2008), Gravity waves in the thermosphere simulated by a general circulation model, *J. Geophys. Res.*, *113*, D01101, doi:10.1029/2007JD008874.

Muschietti, L., and C. T. Dum (1993), Real group velocity in a medium with dissipation, *Phys. Fluids B*, *5*(5), 1383–1397, doi:10.1063/1.860877.

Nimtz, G. (2004), Superluminal signal velocity and causality, *Found. Phys.*, *34*, 1889–1903, doi:10.1007/s10701-004-1625-2.

Oliver, W. L., Y. Otsuka, M. Sato, T. Takami, and S. Fukao (1997), A climatology of F region gravity wave propagation over the middle and upper atmosphere radar, *J. Geophys. Res.*, *102*, 14,499–14,512, doi:10.1029/97JA00491.

Pitteway, M. L. V., and C. O. Hines (1963), The viscous damping of atmospheric gravity waves, *Can. J. Phys.*, *41*, 1935–1948.

Richmond, A. D. (1983), Thermospheric dynamics and electrodynamics, in *Solar-Terrestrial Physics*, edited by R. L. Carovillano and J. M. Forbes, pp. 523–607, D. Reidel, Dordrecht, Holland.

Schubert, G., M. P. Hickey, and R. L. Walterscheid (2003), Heating of Jupiter's thermosphere by the dissipation of upward propagating acoustic waves, *Icarus*, *163*, 398–413, doi:10.1016/S0019-1035(03)00078-2.

Stratton, J. A. (1941), *Electromagnetic Theory*, 333 pp., McGraw-Hill, New York.

Thau, S. A. (1974), Linear dispersive waves, in *Nonlinear Waves*, edited by S. Leibovich and R. Seebass, pp. 44–81, Cornell Univ. Press, Ithaca, N. Y.

Vadas, S. L. (2007), Horizontal and vertical propagation and dissipation of gravity waves in the thermosphere from lower atmospheric and thermospheric sources, *J. Geophys. Res.*, *112*, A06305, doi:10.1029/2006JA011845.

Vadas, S. L., and D. C. Fritts (2004), Thermospheric responses to gravity waves arising from mesoscale convective complexes, *J. Atmos. Sol. Terr. Phys.*, *66*, 781–804, doi:10.1016/j.jastp.2004.01.025.

Vadas, S. L., and D. C. Fritts (2005), Thermospheric responses to gravity waves: Influences of increasing viscosity and thermal diffusivity, *J. Geophys. Res.*, *110*, D15103, doi:10.1029/2004JD005574.

Vadas, S. L., and D. C. Fritts (2009), Reconstruction of the gravity wave field from convective plumes via ray tracing, *Ann. Geophys.*, *27*(1), 147–177.

Volland, H. (1969), The upper atmosphere as a multiple refractive medium for neutral air motions, *J. Atmos. Terr. Phys.*, *31*, 491–514, doi:10.1016/0021-9169(69)90002-6.

Waldock, J. A., and T. B. Jones (1984), The effects of neutral winds on the propagation of medium-scale atmospheric gravity waves at midlatitudes, *J. Atmos. Terr. Phys.*, *46*(3), 217–231, doi:10.1016/0021-9169(84)90149-1.

Walterscheid, R. L. (1997), Simple models of tidal transience: The steady state signal, *J. Geophys. Res.*, *102*(D22), 25,807–25,815, doi:10.1029/97JD02079.

Walterscheid, R. L., and J. H. Hecht (2003), A reexamination of evanescent acoustic-gravity waves: Special properties and aeronomical significance, *J. Geophys. Res.*, *108*(D11), 4340, doi:10.1029/2002JD002421.

Walterscheid, R. L., and M. P. Hickey (2001), One-gas models with height-dependent mean molecular weight: Effects on gravity wave propagation, *J. Geophys. Res.*, *106*, 28,831–28,839.

Walterscheid, R. L., and G. Schubert (1990), Nonlinear evolution of an upward propagating gravity wave: Overturning, convection, transience and turbulence, *J. Atmos. Sci.*, *47*, 101–125, doi:10.1175/1520-0469 (1990)047<0101:NEOAUP>2.0.CO;2.

Walterscheid, R. L., J. H. Hecht, F. T. Djuth, and C. A. Tepley (2000), Evidence of reflection of a long-period gravity wave in observations of the nightglow over Arecibo on May 8–9 1989, *J. Geophys. Res.*, *105*, 6927–6934, doi:10.1029/1999JD901065.

Walterscheid, R. L., G. Schubert, and D. G. Brinkman (2001), Small-scale gravity waves in the upper mesosphere and lower thermosphere generated by deep tropical convection, *J. Geophys. Res.*, *106*, 31,825–31,832, doi:10.1029/2000JD000131.

Yu, Y., and M. P. Hickey (2007), Numerical modeling of a gravity wave packet ducted by the thermal structure of the atmosphere, *J. Geophys. Res.*, *112*, A06308, doi:10.1029/2006JA012092.

M. P. Hickey, Department of Physical Sciences, Embry-Riddle Aeronautical University, 600 S. Clyde Morris Blvd., Daytona Beach, FL 32114, USA.

R. L. Walterscheid, Space Science Applications Laboratory, Aerospace Corporation, MS 260, PO Box 92957, Los Angeles, CA 90009, USA. (richard.walterscheid@aero.org)